Nanoscale

Accepted Manuscript

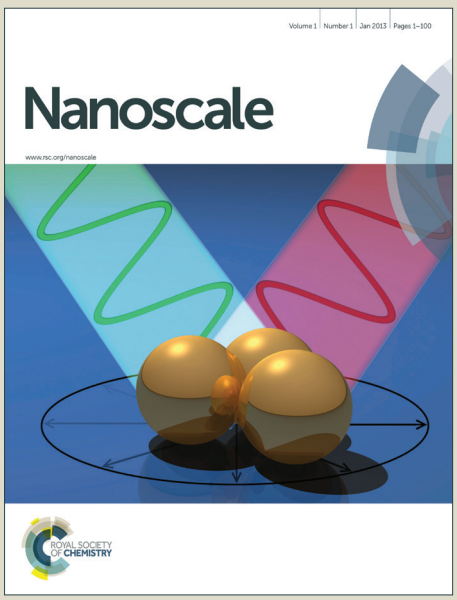

ROYAL SOCIETY OF CHEMISTRY

www.rsc.org/nanoscale

Nanoscale

ARTICLE

Core-decomposition-facilitated fabrication of hollow rare-earth silicate nanowalnuts from core-shell structures via Kirkendall effect†

Received 00th January 20xx,
Accepted 00th January 20xx

DOI: 10.1039/x0xx00000x

www.rsc.org/

Wenli Zhou, ‡[ab] Rui Zou, ‡[a] Xianfeng Yang,[c] Ningyu Huang,[a] Junjian Huang,[a] Hongbin Liang,[a] and Jing Wang*[a]

Hollow micro-/nanostructures have been widely applied in the fields of lithium ion batteries, catalysis, biosensing, biomedicine, and so forth. Kirkendall effect, which involves in a non-equilibrium mutual diffusion process, is one of many important fabrication strategies for the formation of hollow nanomaterials. Accordingly, fully understanding of the interdiffusion process at the nanoscale is very important for the development of novel multifunctional hollow materials. In this work, hollow Y_2SiO_5 nanowalnuts have been fabricated from the conversion of $YOHCO_3$@SiO_2 core-shell nanospheres via the Kirkendall effect. More importantly, it was found that in the conversion process, the decomposition of $YOHCO_3$ core imposes on the formation of the Y_2SiO_5 interlayer by facilitating the initial nucleation of the Kirkendall nanovoids and accelerating the interfacial diffusion of Y_2O_3@SiO_2 core@shell. The simple concept developed herein can be employed as a general Kirkendall effect strategy without assistant of any catalytically active Pt nanocrystals or gold motion for future fabrication of novel hollow nanostructures. Moreover, the photoluminescence properties of rare-earth ions doped hollow Y_2SiO_5 nanoparticles are researched.

Introduction

Hollow micro-/nanostructures for their variety of applications, such as lithium ion batteries, catalysis, sensing, and biomedicine, and so forth, have widely attracted interests and investigations in many current and emerging areas of technology.[1] In the past decades, considerable efforts have been made in controllable fabrication of the hollow structures.[2] Recently, a new concept of "Kirkendall effect" has emerged as an alternative approach to fabricate hollow nanostructures.[3] This approach normally refers to a non-equilibrium mutual diffusion process through the interface of coupled materials.[1b, 4] Generally, regarding the development of the hollow interior, it is expected that a bulk diffusion/reaction process dominates the generation of nanoscale Kirkendall voids by initial intersection of the core and shell at the interface and subsequent outward diffusion of the core component along the surface of grown voids (surface diffusion).[5] Yin et al. for the first time reported the formation of hollow cobalt sulfide nanocrystals from cobalt nanocrystals in solution with sulfur based on the nanoscale Kirkendall effect.[6] Since then, the fabrication of hollow micro-/nanostructures via this effect has been extensively researched.[3b, 7] At present, these researches mainly involve in two kinds of structures: one is hollow nanoparticle, such as iron-, cobalt-, nickel- and copper-compounds;[8] another is one dimensional nanotube, including binary and ternary compounds.[9] These hollow compounds are generally transformed from either solid-gas or solid-solution or solid-solid reaction. However, the transformation mechanism and reaction kinetics still remain a great challenge.

Recently, Ha et al. found reversible and cyclical transformations between core@shell and hollow nano-structures in confined reactions of MnO and SiO_2 within nanosized spheres. The transformations complete under the assistance of catalytically active Pt nanocrystals and depend on the gas environment.[10] More previously, Yang reported outward diffusion of Au interlayer in ZnO-Au-SiO_2 sandwich nanowires can facilitate the fabrication of Zn_2SiO_4 nanotubes.[11] During the transformation process, the gold motion facilitates the nucleation of the Kirkendall voids at multiple positions, and the kinetically-favoured surface diffusion subsequently accelerates the formation of a Zn_2SiO_4 nanotube. These researches disclose that the nucleation of nanoscale Kirkendall voids at the beginning is vital to the formation of hollow nanostructures. Inspired by this, we assume that it is

[a] Ministry of Education Key Laboratory of Bioinorganic and Synthetic Chemistry, State Key Laboratory ofOptoelectronic Materials and Technologies, KLGHEI of Environment and Energy Chemistry, School of Chemistry and Chemical Engineering, Sun Yat-sen University, Guangzhou, Guangdong 510275, China. E-mail: ceswj@mail.sysu.edu.cn.
[b] College of Chemistry and Chemical Engineering, Hunan Normal University, Changsha, Hunan 410081, China
[c] Analytical and Testing Center, South China University of Technology, Guangzhou, 510640, China.

† Electronic Supplementary Information (ESI) available: Refined XRD patterns of other control experiments, including using Y_2O_3@SiO_2 instead of $YOHCO_3$@SiO_2 to synthesize hollow Y_2SiO_5 NPs; EDX spectrum of hollow Y_2SiO_5 nanowalnuts. See DOI: 10.1039/x0xx00000x

‡ Wenli Zhou and Rui Zou contributed equally to this work.

possible for the decomposition of cores during annealing to facilitate the reaction of producing hollow micro-/nanostructures. The reasons are that the decomposition temperature of core is generally below the core-shell reaction temperature and the decomposition of core could cause large interfacial void surface for the core to diffusion into the shell at the beginning. In order to confirm this hypothesis, we select $YOHCO_3$@SiO_2 core@shell nanostructure as a precursor to investigate its transformation process at elevated temperature and the formation mechanism of hollow Y_2SiO_5 nanocrystals. The reasons why we choose hollow Y_2SiO_5 nanocrystals as an example to investigate whether the decomposition of cores during annealing facilitates the reaction of producing hollow micro-/nanostructures includes: (i) preparing uniform $YOHCO_3$ cores and then coating SiO_2 can be done easily, (ii) $YOHCO_3$ cores can decompose during thermal treatment and simultaneously form new contractive Y_2O_3 cores, (iii) the fluidity of solid state SiO_2 shells is limited at temperatures given in this case far below its melting point, (iv) the resulted Y_2SiO_5 is a famous host material for rare-earth ions doping.

Fortunately, we successfully synthesized monodisperse hollow Y_2SiO_5 nanowalnuts simply by heating the $YOHCO_3$@SiO_2 core@shell nanostructure at elevated temperature, which benefits from the Kirkendall effect. The transformation mechanism, especially, how the decomposition of core ($YOHCO_3$ in this case) influences the thermal diffusion behavior of Y_2O_3@SiO_2 core@shell without assistant of any catalytically active Pt nanocrystals or gold motion, was systematically investigated. The strategy developed herein is expected to provide a general route for the fabrication of novel hollow and porous nanostructures in the future. Moreover, the photo-luminescence properties of rare-earth ions doped Y_2SiO_5 nanoparticles are studied.

Experimental section

Synthesis of $YOHCO_3$ and Y_2O_3 core nanoparticles

$YOHCO_3$ nanoparticles were prepared according to a literature procedure.[12] Firstly, proper amounts of Y_2O_3 was dissolved in dilute nitric acid to make a nitrate solution. The concentration of Y^{3+} was kept at 0.2 M. 6.0072 g $(NH_2)_2CO$ powder was dissolved in 250 ml water solution in a 500 ml three-neck round-bottom flask. Subsequently, a 10 ml $Y(NO_3)_3$ solution was added and stirred for 30 min. The resulting mixture was then heated at 96 °C and kept for 1 h before cooling down to room temperature. The as-prepared nanoparticles were collected by centrifugation and washed with water and ethanol for several times. After rinsing, the precursor was dried at 60 °C for 12 h. Y_2O_3 core NPs were obtained by annealing $YOHCO_3$ at 700 °C for 2 h in a muffle furnace in air. The Ce^{3+} and Tb^{3+} co-doped $YOHCO_3$ cores were synthesized in a similar homogenous precipitation procedure, except for partial replacement of Y^{3+} by Ce^{3+} and Tb^{3+} ions.

Synthesis of $Y(OH)CO_3$@SiO_2 and Y_2O_3@SiO_2 core@shell

Coating SiO_2 was carried out by hydrolysis of tetraethoxysilane (TEOS).[13] Firstly, 0.05 g $Y(OH)CO_3$ or Y_2O_3 core NPs were dispersed in 24 ml ethanol by sonication for 2 h. Then 1.44 ml ammonia (30 wt% purity) and 0.6 ml TEOS was added, and stirred for 4 h at room temperature. Here, ammonia was used to catalyze the hydrolysis and condensation reactions of TEOS during the SiO_2 coating process. The core-shell nanoparticles were also collected by centrifugation and washed with water and ethanol for several times. After this, the product was dried at 60 °C for 12 h.

Synthesis of hollow rare-earth silicate nanoparticles

Annealing treatments of the core@shell NPs were performed at 900 – 1000 °C in air for different time, with a temperature-raised rate of 2 °C/min.

Characterization

The solid products were characterized using powder x-ray diffraction (XRD, Rigaku D/MAX 2200 VPC) at a scanning rate of 10 °/min, with Cu Kα1 radiation (λ = 1.5405 Å). Structural refinement of XRD data was performed using the TOPAS-Academic program.[14] The morphology and structure of the as-prepared products were inspected using scanning electron microscopy (SEM, FEI Quanta 400). Transmission electron microscopy (TEM), high-resolution TEM (HRTEM) and selected area electron diffraction (SAED) analyses were performed on a JEOL 2010 instrument. Images were acquired digitally on a Gatan multipole CCD camera. Thermogravimetric-differential thermal analysis (TG-DTA) curves were recorded on Thermogravimetry Analyzer (NetzschTG-209). Photoluminescence excitation (PLE) and emission (PL) spectra were determined on a FSP920-combined Time Resolved and Steady State Fluorescence Spectrometer (Edinburgh Instruments) with a 450 W xenon lamp as the excitation source. The quantum efficiency was collected using integrating sphere.

Results and discussion

Preparation and characterization of hollow Y_2SiO_5 nanoparticles

Uniform monodisperse $YOHCO_3$ nanoparticles (NPs) were grown by homogeneous precipitation method.[12] From the SEM image shown in Fig. 1a, the diameter of the $YOHCO_3$ NPs is about 230 nm. A close view reveals that the as-prepared $YOHCO_3$ NPs have a quite smooth surface. The electron diffraction pattern suggests the NPs are amorphous (the inset in Fig. 1a). After coating SiO_2 shells on $YOHCO_3$ NPs through the modified Stöber method, [13b] the $YOHCO_3$@SiO_2 core-shell structures were obtained as shown in TEM micrographs (Fig. 1b). The magnified TEM image (the inset in Fig. 1b) shows the thickness of the SiO_2 shell is about 35 nm and the whole core-shell particle is about 300 nm in diameter.

Fig. 2 shows the SEM and TEM micrographs of as-fabricated hollow NPs through sintering the $YOHCO_3$@SiO_2 core@shell structures at 1000 °C for different time. In order to moreclearly observe the surface of the silicate products, the

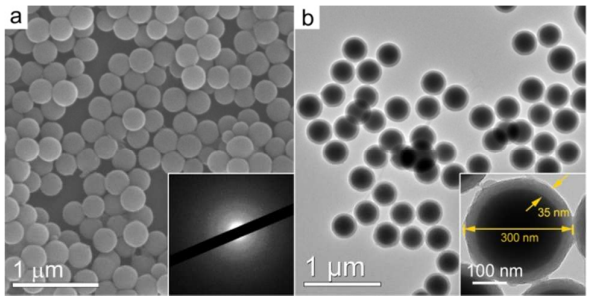

Fig. 1 (a) SEM image of $YOHCO_3$ nanospheres, the inset shows their ED pattern, (b) TEM image of $YOHCO_3$@SiO_2 core-shell structures, the inset shows the magnified TEM image.

thermally treated core-shell structures were soaked in 1 M NaOH for 12 h to remove the unreacted SiO_2 shell. The SEM results show that the products look like walnuts with uniform size (about 230 nm) and coarse surface. Some cracked nanowalnuts, induced by ultrasound, present partly hollow or completely hollow inner structure (the insets of Fig. 2a, c, e and g). Further, TEM technology was employed to fully exhibit the inner structure of the as-annealed products. For the samples annealed for 0.5 h, the inner of nanowalnuts shows an incompletely hollow feature, as shown in Fig. 2b. The black bulks (marked with yellow arrows) in the inner of nanowalnuts should be the unreacted Y_2O_3 according to the refined XRD results (Fig. S1†). With the reaction time increasing, the amount of unreacted Y_2O_3 bulks decreases (Fig. 2d, f), which is consistent with the XRD results (Fig. S1†).

High resolution (HR) TEM image (Fig. 3a) taken from a selected hollow nanowalnut (obtained at 1000 ^{o}C for 6 h) at the edge shows that the interplanar spacing of 0.54 nm corresponds to the (200) planes of Y_2SiO_5. Furthermore, its selected area electron diffraction (SAED) pattern (Fig. 3b) exhibits a multicrystalline feature and can be indexed to the monoclinic structure of Y_2SiO_5. The elemental mapping of Y, Si and O (Fig. 3d-g) reveals all the three elements almost distribute in the shell instead of in the inner, directly indicating Y_2SiO_5 nanoparticle is hollow. In addition, energy-dispersive X-ray (EDX) spectroscopy was employed to characterize the elemental composition of the as-prepared hollow Y_2SiO_5 nanowalnuts (Fig. S2†), and the results confirm the existence of the elements Y, Si, and O with an atomic ratio of 3:2:5.When the reaction time was prolonged up to 12 h, the $YOHCO_3$@SiO_2 core-shell structures were completely converted into hollow silicates nanowalnuts. The thickness and the inner diameter of as-obtained hollow silicate nanowalnuts are estimated to be about 40 nm and 200 nm, which are close to the thickness (35 nm) of SiO_2 shell and the diameter (230 nm) of the $YOHCO_3$ core, respectively. Similar to the formations of some hollow nanostructures, for example, hollow Zn_2SiO_4 nanotubes from the conversion of ZnO@SiO_2,[15] the formation of hollow Y_2SiO_5 nanowalnuts represents an extreme case of Kirkendall effect. As shown in Fig. 1 and Fig. 2, the whole nanostructures show slight shrink from 300 to 280

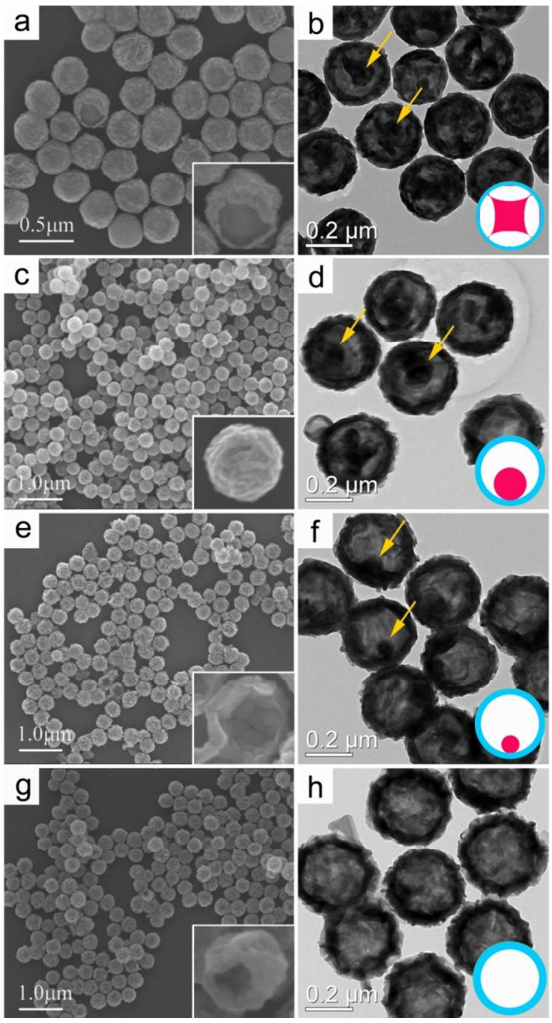

Fig. 2 SEM and TEM images of the post-treated $YOHCO_3$@SiO_2 core-shell structures sintered at 1000 °C for different time, (a, b) 0.5 h, (c, d) 3 h, (e, f) 6 h and (g, h) 12 h.

nm and an unobvious thickness change from 35 to 40 nm. This indicates that the outward diffusion rate of active Y_2O_3 cores from the precursor $YOHCO_3$ is significantly larger than the inward diffusion rate of SiO_2 shells, which plays a key role in the formation of hollow nanostructures.

In order to study the chemical conversion process from $YOHCO_3$@SiO_2 core-shell into hollow Y_2SiO_5 NPs, the TG-DTA curves (Fig. 4) and XRD patterns (Fig. 5) were recorded. The weight loss percentage (Fig. 4, curve a) of $YOHCO_3$ precursors below 750 °C is estimated to be about 34.0%, which is close to the theoretical value of 32.0%. These results suggest the $YOHCO_3$ are decomposed into Y_2O_3 (solid), H_2O (gas) and CO_2 (gas) below 750 ^{o}C. Additionally, the weight loss percentage (Fig. 4, curve b) of $YOHCO_3$@SiO_2 is evaluated to be about 20.2%, based on which the mass fraction of SiO_2 and Si:Y ratio are calculated to be about 37.5% and 1.66:1, respectively. Since the molar ratio of SiO_2:Y_2O_3 here is larger than 1, the SiO_2

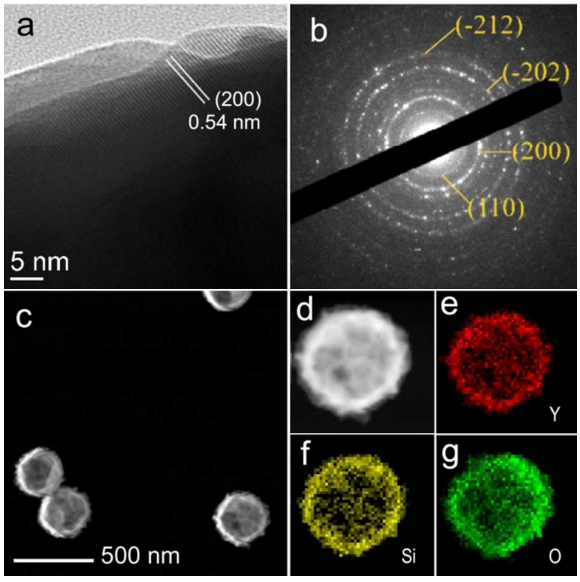

Fig. 3 HRTEM image (a) and SAED pattern (b) of hollow Y_2SiO_5 nanostructures obtained from $YOHCO_3$@SiO_2 core-shell nanostructures annealed at 1000 °C for 6 h. HAADF-STEM (c-g) elemental distribution maps.

shell would be excess and further react with the target Y_2SiO_5 to form other impurity phases. At 750 - 1050 °C (Fig. 4c, d),$YOHCO_3$@SiO_2 precursor presents an extreme exothermic peak relative to $YOHCO_3$, contributing to the reaction of Y_2O_3 core and SiO_2 shell. Accordingly, the temperature for the reaction process of Y_2O_3 core and SiO_2 shell were set at 1000 °C for different time to systematically investigate the phase translation by XRD patterns of the as-annealed samples from $YOHCO_3$@SiO_2 core@shell nanostructures. For 0.5 h (Fig. 5a), the $YOHCO_3$@SiO_2 core@shell is transformed to the mixture of Y_2SiO_5 and Y_2O_3, indicating $YOHCO_3$ is initially decomposed into Y_2O_3, and the Y_2O_3 core subsequently reacts with the SiO_2 shell and finally Y_2SiO_5 forms. As the reaction time increases up to 3 h (Fig. 5b) and 6 h (Fig. 5c), the relative diffraction intensity of Y_2SiO_5 phase increases and that of Y_2O_3 contrarily decreases. For 9 h (Fig. 5d), the Y_2O_3 core nearly disappears and another silicate $Y_2Si_2O_7$ phase appears. While for 12 h (Fig. 5e), the XRD pattern of product is fully indexed to the $Y_2Si_2O_7$ phase. These results above are strongly supported by the weight loss percentage (Fig. 4, curve b) of $YOHCO_3$@SiO_2. These results mentioned above also reveal that to modify the thickness of SiO_2 shell and the sintering condition can control the final silicate species or phase.

In summary, the collected XRD patterns and TG-DTA curves suggest that the conversion reaction of $YOHCO_3$@SiO_2 core@shell structures mainly contains three steps: (1) $2YOHCO_3 \rightarrow Y_2O_3 + H_2O\uparrow + 2CO_2\uparrow$, (2) $Y_2O_3 + SiO_2 \rightarrow Y_2SiO_5$ and (3) $Y_2SiO_5 + SiO_2 \rightarrow Y_2Si_2O_7$. In order to depict the reaction rate between Y_2O_3 cores and SiO_2 shells, we estimate the percentages of Y_2O_3 and Y_2SiO_5 content in hollow nanowalnuts sintered at 1000 °C for different reaction time (0 - 6 h) with

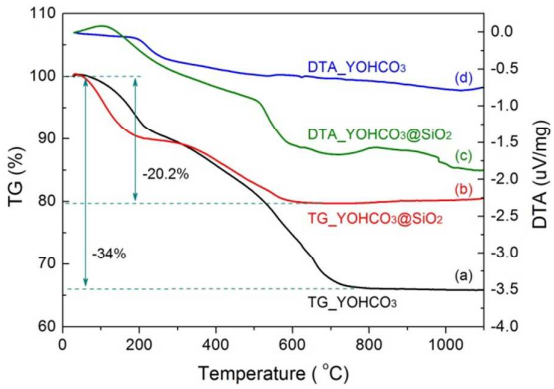

Fig. 4 TG-DTA curves of $YOHCO_3$ nanospheres and $YOHCO_3$@SiO_2 core-shell nanostructures.

Rietveld refinement method (Fig. S1†). The percentage as a function of reaction time (0 – 6 h) is plotted in Fig. 5f. Clearly, when the reaction time is only for 0.5 h, the percentage of Y_2SiO_5 content is highly up to 91.57%. As the reaction time increases from 0.5 h to 3 h and 6 h, the percentage shows a slight increase (91.57% → 95.56% → 97.09%). This trend reveals that the reaction rate of Y_2SiO_5 is initially very rapid and becomes slow later. These results suggest that the outward diffusion rate of Y_2O_3 does not keep constant during the conversion process. Since the outward diffusion rate of Y_2O_3 is related to the Kirkendall voids of Y_2O_3 cores, one can conclude that the initial nucleation of the Kirkendall voids principally determines the whole reaction rate.[5a, 16]

Formation Mechanism of Hollow Y_2SiO_5 Nanoparticles

In order to understand the role of the decomposition of $YOHCO_3$ cores in the formation process of hollow Y_2SiO_5 nanoparticles, the reaction process of Y_2O_3@SiO_2 and $YOHCO_3$@SiO_2 annealed at 900 °C were comparatively investigated based on the TEM images (Fig. 6) and XRD patterns (Fig. 7 and Fig. S1†). The Y_2O_3@SiO_2 core@shell nanostructure was synthesized by a two-step strategy. Firstly, the $YOHCO_3$ nanospheres was annealed at 700 °C for 2 h to obtain the Y_2O_3 nanospheres and the later was then coated with SiO_2 shell. After Y_2O_3@SiO_2 core@shell nanostructures were annealed at 900 °C for 0.5 h, some isolated nanovoids appear and distribute at the positions close to the entire interface (Fig. 6a – c) . The formation of nanoscale Kirkendall voids were due to bulk diffusion process of Y_2O_3@SiO_2. And the percentage of Y_2SiO_5 is estimated to be 21.52% based on the analysis of its XRD pattern (Fig. 7a). When the reaction time is up to 3 h, many nanoscale Kirkendall voids aggregate into bigger ones, which are readily detected in the inner of the core–shell remainders (Fig. 6d). Meanwhile, the X-ray diffraction intensity of Y_2SiO_5 products correspondingly increases and the percentage of Y_2SiO_5 is estimated to be 39.04% (Fig. 7b). Based on these results discussed above, we assume that the Y_2O_3–SiO_2 solid–solid reaction, driven by the bulk diffusion process, proceeds very slowly even at 900 °C.

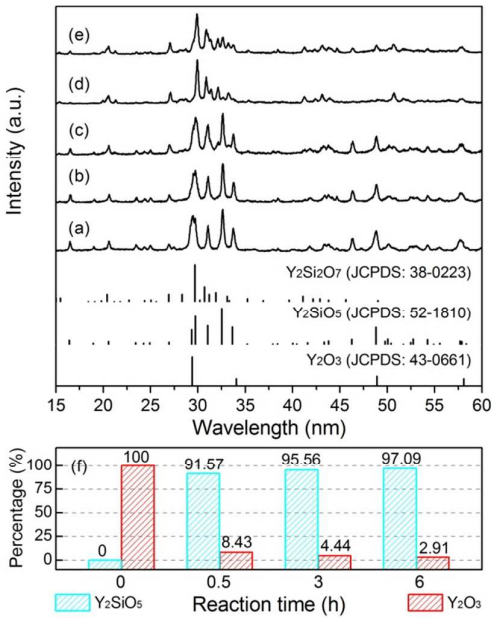

Fig. 5 XRD patterns of the as-annealed samples from $YOHCO_3$@SiO_2 core@shell nanostructures sintered at 1000 °C for different time, (a) 0.5 h; (b) 3 h; (c) 6 h; (d) 9 h, (e) 12 h. (f) The percentages of Y_2O_3 and Y_2SiO_5 content in hollow nanowalnuts sintering at 1000 °C for different reaction time (0 – 6 h).

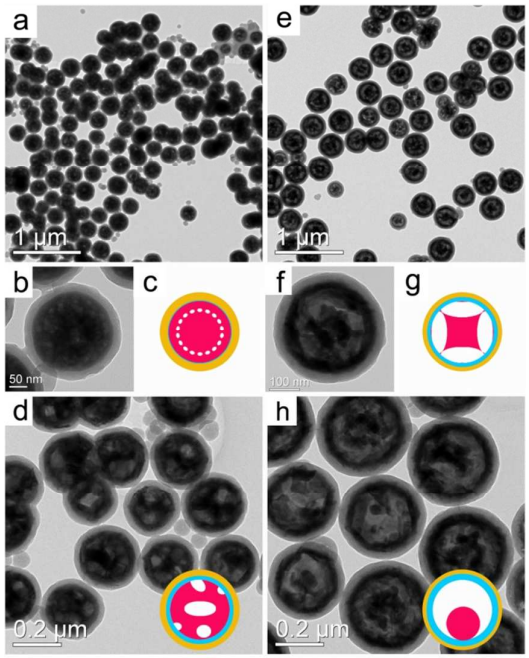

Fig. 6 TEM images of hollow nanospheres formed by annealing core@shell nanostructures at 900 °C in air. (a - c) Y_2O_3@SiO_2 for 0.5 h; (d) Y_2O_3@SiO_2 for 3 h; (e - g) $YOHCO_3$@SiO_2 for 0.5 h; (h) $YOHCO_3$@SiO_2 for 3 h.

The slow reaction rate can be attributed to the high bond energy of SiO_2 as well as the limited supply of activated Y^{3+} ions. Therefore, an extremely long time is required for the widespread nucleation of the initial Kirkendall voids. Once a large void preferentially shapes at the Y_2O_3–SiO_2 interface, hollow nanostructure would rapidly develop from this gap by kinetically-favoured surface diffusion.

Comparatively, the reaction process of $YOHCO_3$@SiO_2 is much different with Y_2O_3@SiO_2 under the same annealing conditions. After annealed at 900 °C for 0.5 h, it is clearly seen in Fig. 6e - g that there exist many bridge-like linkages between the residual Y_2O_3 core and the Y_2SiO_5 interlayer. From the refined XRD results as shown in Fig. 7, the percentage of Y_2SiO_5 are estimated to be 73.90% and 87.02% for $YOHCO_3$@SiO_2 for 0.5 h and 3 h, which are greatly larger than 21.52% and 39.04% for Y_2O_3@SiO_2 for 0.5 h and 3 h, respectively. This finding readily reveals that the decomposition of $YOHCO_3$ cores can facilitate the formation of hollow Y_2SiO_5 nanoparticles. Owing to the simultaneous occurrence of gas (H_2O + CO_2) outward diffusion/escape accompanying the decomposition of $YOHCO_3$, some nanoscale Kirkendall voids form at Y_2O_3-SiO_2 core-shell interface. Once these voids grow to a certain size, the as-formed Y_2O_3 core will dominantly diffuse outward into the SiO_2 shell along the pore surface, because the activation energy of the surface diffusion (Q_S = 187 kJ/mol) of Y_2O_3 is lower than that of the bulk diffusion (Q_B = 191 kJ/mol).[17] Therefore, the decomposition of $YOHCO_3$ cores initially induces the rapid growth of the Kirkendall nanovoids and consequently facilitates the formation of Y_2SiO_5 interlayer. When the reaction time prolongs up to 3 h, the remaining Y_2O_3 core shrinks and the voids grow bigger (Fig. 6h). The XRD results (Fig. 7d) show that the percentage of Y_2SiO_5 increases slightly from 73.90% (0.5 h) up to 87.02% (3 h), indicating the reaction rate decreases. The decreasing reaction rate is mainly due to the decreasing surface diffusion rate that is caused by the decreasing surface area of Y_2O_3 or the decreasing amount of remaining Y_2O_3 as the reaction time prolongs. Additionally, the formation of Y_2SiO_5 from $YOHCO_3$@SiO_2 is also more rapid than from Y_2O_3@SiO_2 annealed at 950 °C for 3 h (Fig. S3†). Therefore, it is reasonable to suggest that the formation of the hollow Y_2SiO_5 nanoparticles from the $YOHCO_3$@SiO_2 core–shell nanostructures is actually triggered by a few preferentially generated interfacial voids due to the decomposition of $YOHCO_3$ core.

The annealing temperatures far below the melting point of SiO_2 make its fluidity limited. Accordingly, it is supposed that some vacancies induced by the decomposition of the $YOHCO_3$ cores failed to be compensated. These frozen vacancies would possibly fuse into large voids during annealing, some of which gathered at the Y_2O_3-SiO_2 core-shell interface. Abundant defects and weakened bonds would be produced in the interfacial SiO_2 in contrast to the annealing process of Y_2O_3@SiO_2 precursor. Therefore, it can be inferred that the decomposition of $YOHCO_3$ cores introduces additional vacancies, voids and defects into the interface of Y_2O_3-SiO_2 nanoparticle, which facilitates the nucleation of nanoscale

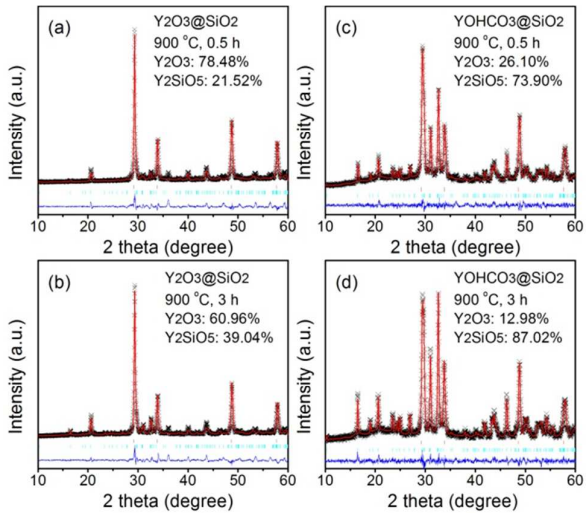

Fig. 7 Refined XRD patterns of products from annealing (a, b) Y_2O_3@SiO_2 and (c, d) $YOHCO_3$@SiO_2 core-shell structures at 900 °C for (a, c) 0.5 h and (b, d) 3 h, respectively.

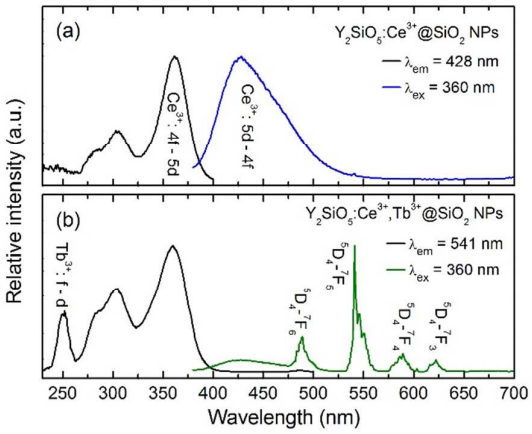

Fig. 8 Photoluminescence excitation and emission spectra of (a) Y_2SiO_5:Ce^{3+}@SiO_2 and (b) Y_2SiO_5:Ce^{3+}, Tb^{3+}@SiO_2 nanoparticles.

Kirkendall voids at multiple positions. Once this initial void nucleation is adequately achieved, the Y_2O_3 core could rapidly diffuse into the SiO_2 shell along the interfacial void surfaces. Therefore, the formation of Y_2SiO_5 is accelerated. As for Y_2O_3@SiO_2 core-shell nanoparticles, only by kinetically-disfavored bulk diffusion can nanoscale Kirkendall voids form at the initial stage, therefore the large voids need long time to be produced, leading to a slow reaction forming Y_2SiO_5 interlayer. The above procedures proposed for the formation of the hollow Y_2SiO_5 nanoparticles are shown in Scheme 1.

Photoluminescence Properties of Hollow Y_2SiO_5:Ce^{3+},Tb^{3+}@SiO_2 Nanoparticles

Considering the potential applications of the hollow NPs in the field of biomedical imaging, biosensing and drug delivery, and so forth,[18] we researched the photo luminescence properties

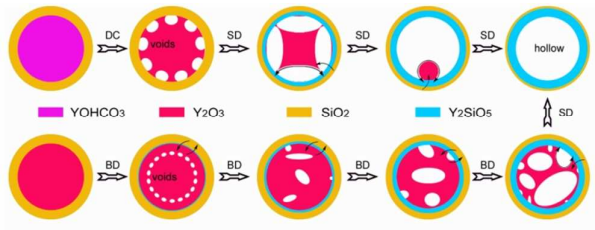

Scheme 1 The hollow Y_2SiO_5 nanoparticles are transformed from $YOHCO_3$@SiO_2 and Y_2O_3@SiO_2 core-shell structures via Kirkendall effect. The transformation process can be facilitated through the decomposition of core. DC: decomposition, SD: surface diffusion, BD: bulk diffusion, black solid arrow: interdiffusion between Y_2O_3 core and SiO_2 shell.

of rare-earth ions doped hollow Y_2SiO_5@SiO_2 NPs. The EDX spectrum of 1%Ce^{3+}-9%Tb^{3+} co-doped sample shows the existence of elemental Y, Ce, Tb, Si and O and the atomic ratio of Y, Ce and Tb is estimated to be 18.49: 0.24: 2.11, which is very closed to the nominal composition of 90: 1: 9 (Fig. S4†). Fig. 8 shows the PLE and PL spectra of 1%Ce^{3+} singly- and 1%Ce^{3+}-9%Tb^{3+} co-doped hollow NPs. The Y_2SiO_5:1%Ce^{3+}@SiO_2 NPs present a broad blue emission band peaking around 428 nm under UV-light excitation of 360 nm (Fig. 8a). It is well known that photoluminescence properties of Ce3+ strongly depend on its local lattice environment. As shown in Fig. S5 and Fig. 8a, free Ce^{3+} ion in nitrate solution shows much different spectral characteristic with Ce^{3+} ion in hollow Y_2SiO_5 nanoparticles. The latter shows almost the same spectral characteristic with bulk Y_2SiO_5 matrix[19]. These results indicate that Ce^{3+} ion actually enter Y_2SiO_5 matrix and occupy the Y cation site instead of in solution or SiO_2 shell. When some Tb^{3+} are co-doped into the hollow NPs, the blue emission intensity of Ce^{3+} remarkably decreases and green emissions of Tb^{3+} (486, 541, 584, 623 nm) appear under the excitation of Ce^{3+} ions at 360 nm (Fig. 8b). Monitoring the emission ($^5D_4 \rightarrow {}^7F_5$) of Tb^{3+} at 541 nm,[20] the excitation spectrum contains a weak band at about 300 nm and a strong band dominating at 360 nm, both of which are ascribed to 4*f*→5*d* transitions of Ce^{3+},[21] and the band around 250 nm should be attributed to 4*f*→5*d* transition of Tb^{3+}. The presence of the 4*f*→5*d* transitions of Ce^{3+} in the excitation spectrum of Tb^{3+} indicates that an energy transfer from Ce^{3+} to Tb^{3+} occurs in the hollow sample. The decay curves show that decay time of Ce^{3+} decreases from 36.89 ns to 24.24 ns before and after Tb3+ ion was co-doped (Fig. S6†). The result further prove the existence of energy transfer from Ce^{3+} to Tb^{3+} in hollow Y_2SiO_5:Ce^{3+}, Tb^{3+}@SiO_2 NPs.[19] These photoluminescence properties of Ce^{3+} and Tb^{3+} and the EDX result (Fig. S4†) of Y_2SiO_5: Ce^{3+}, Tb^{3+} NPs suggest that Ce and Tb elements have been indeed doped into the matrix lattice to occupy the Y lattice site. Additionally, the internal quantum

efficiency of $Y_2SiO_5:Ce^{3+},Tb^{3+}@SiO_2$ NPs is estimated to be 14% using integrating sphere.

Conclusions

In summary, a hollow Y_2SiO_5 nanostructure was successfully fabricated through a homogenous precipitation-Stöber-heating three steps strategy. The first two steps, i.e., homogenous precipitation/Stöber, is to construct $YOHCO_3@SiO_2$ core-shell structure. Thereafter, the hollow Y_2SiO_5 nanoparticles are transformed from the $YOHCO_3@SiO_2$ core-shell structures by outward diffusion of the as-decomposed active Y_2O_3 core into the SiO_2 shell at high temperatures via Kirkendall effect, which plays a key role in synthesizing hollow Y_2SiO_5 nanoparticles. More importantly, on the basis of the comparison of transformation processes of $YOHCO_3@SiO_2$ and $Y_2O_3@SiO_2$ core@shell into hollow Y_2SiO_5, we find that the decomposition of $YOHCO_3$ cores can facilitate the initial nucleation of the nanoscale Kirkendall voids and consequently influence the Y_2O_3-SiO_2 core-shell interface, which accelerates the formation of the Y_2SiO_5 interlayer. We believe that the strategy for hollow Y_2SiO_5 nanostructure developed herein can be expected as a general route for the fabrication of novel hollow and porous nanostructures in the future.

Acknowledgements

This work was financially supported by the "973" programs (2014CB643801), the NSFC (21271191), the Joint Funds of the National Natural Science Foundation of China and Guangdong Province (U1301242), Teamwork Projects of Guangdong Natural Science Foundation (S2013030012842), Guangdong Provincial Science & Technology Project (2013B090800019 and 2013Y2-00118), Natural Science Foundation of Guangdong Province (2014A030313114), and the Fundamental Research Funds for the Central Universities (14lgqt02).

Notes and references

1 (a) L. Zhang, H. B. Wu, S. Madhavi, H. H. Hng and X. W. Lou, *J. Am. Chem. Soc.,* 2012**, 134**, 17388; (b) W. Wang, M. Dahl and Y. Yin, *Chem. Mater.,* 2013**, 25**, 1179; (c) J. Zhang, Y. Wang, Z. Xu, H. Zhang, P. Dong, L. Guo, F. Li, S. Xin and W. Zeng, *J. Mater. Chem. B,* 2013**, 1**, 330; (d) X. W. Lou, L. A. Archer and Z. C. Yang, *Adv. Mater.,* 2008**, 20**, 3987; (e) W. Wei, L.-X. Song and L. Guo, *Chin. Chem. Lett.,* 2015**, 26**, 124.

2 (a) J. Liu, G. Zhang, J. C. Yu and Y. Guo, *Dalton Trans.,* 2013**, 42**, 5092; (b) L. Zhang, H. B. Wu and X. W. Lou, *J. Am. Chem. Soc.,* 2013**, 135**, 10664; (c) J. Nai, Y. Tian, X. Guan and L. Guo, *J. Am. Chem. Soc.,* 2013**, 135**, 16082.

3 (a) H. J. Fan, U. Gosele and M. Zacharias, *Small,* 2007**, 3**, 1660; (b) J. G. Railsback, A. C. Johnston-Peck, J. W. Wang and J. B. Tracy, *ACS Nano,* 2010**, 4**, 1913.

4 A. Paul, M. J. H. van Dal, A. A. Kodentsov and F. J. J. van Loo, *Acta Mater.,* 2004**, 52**, 623.

5 (a) H. J. Fan, M. Knez, R. Scholz, D. Hesse, K. Nielsch, M. Zacharias and U. Gosele, *Nano Lett.,* 2007**, 7**, 993; (b) K. N. Tu and U. Gosele, *Appl. Phys. Lett.,* 2005**, 86**, 093111.

6 Y. D. Yin, R. M. Rioux, C. K. Erdonmez, S. Hughes, G. A. Somorjai and A. P. Alivisatos, *Science,* 2004**, 304**, 711.

7 F. Zhang, Y. F. Shi, X. H. Sun, D. Y. Zhao and G. D. Stucky, *Chem. Mater.,* 2009**, 21**, 5237; (b) M. Sasidharan, N. Gunawardhana, M. Inoue, S.-i. Yusa, M. Yoshio and K. Nakashima, *Chem. Commun.,* 2012**, 48**, 3200; (c) B. D. Anderson and J. B. Tracy, *Nanoscale,* 2014**, 6**, 12195; (d) Y. Yu, X. Yin, A. Kvit and X. Wang, *Nano Lett.,* 2014**, 14**, 2528; (e) J. Lian, K. Anggara, M. Lin and Y. Chan, *Small,* 2014**, 10**, 667.

8 (a) N. Yan, Q. Chen, F. Wang, Y. Wang, H. Zhong and L. Hu, *J. Mater. Chem. A,* 2013**, 1**, 637; (b) R. M. Ding, J. P. Liu, J. Jiang, Y. Y. Li, Y. Y. Hu, X. X. Ji, Q. B. Chi, F. Wu and X. T. Huang, *Chem. Commun.,* 2009, 4548; (c) J. Kou, A. Saha, C. Bennett-Stamper and R. S. Varma, *Chem. Commun.,* 2012**, 48**, 5862; (d) Y. Lu, J.-p. Tu, Q.-q. Xiong, H. Zhang, C.-d. Gu, X.-l. Wang and S. X. Mao, *CrystEngComm,* 2012**, 14**, 8633; (e) Z. Yang, N. Yang, J. Yang, J. Bergström and M.-P. Pileni, *Adv. Funct. Mater.,* 2015**, 25**, 891.

9 (a) M. H. Park, Y. Cho, K. Kim, J. Kim, M. L. Liu and J. Cho, *Angew. Chem. Int. Ed.,* 2011**, 50**, 9647; (b) D. R. Cummins, H. B. Russell, J. B. Jasinski, M. Menon and M. K. Sunkara, *Nano Lett.,* 2013**, 13**, 2423; (c) S. R. Chun, W. A. Sasangka, M. Z. Ng, Q. Liu, A. Du, J. Zhu, C. M. Ng, Z. Q. Liu, S. Y. Chiam and C. L. Gan, *Small,* 2013**, 9**, 2546; (d) Y. Yang, D. S. Kim, R. Scholz, M. Knez, S. M. Lee, U. Gösele and M. Zacharias, *Chem. Mater.,* 2008**, 20**, 3487; (e) H. M. Chen, C. K. Chen, R.-S. Liu, C.-C. Wu, W.-S. Chang, K.-H. Chen, T.-S. Chan, J.-F. Lee and D. P. Tsai, *Adv. Energy Mater.,* 2011**, 1**, 742.

10 T.-L. Ha, J. G. Kim, S. M. Kim and I. S. Lee, *J. Am. Chem. Soc.,* 2013**, 135**, 1378.

11 Y. Yang, R. B. Yang, H. J. Fan, R. Scholz, Z. P. Huang, A. Berger, Y. Qin, M. Knez and U. Gosele, *Angew. Chem. Int. Ed.,* 2010**, 49**, 1442.

12 X. Qin, G. Zhou, H. Yang, Y. Yang, J. Zhang and S. Wang, *J. Alloys Compd.,* 2010**, 493**, 672.

13 (a) R. Martin-Rodriguez, R. Valiente, C. Pesquera, F. Gonzalez, C. Blanco, V. Potin and M. C. M. de Lucas, *J. Lumin.,* 2009**, 129**, 1109; (b) C. Hui, C. Shen, J. Tian, L. Bao, H. Ding, C. Li, Y. Tian, X. Shi and H.-J. Gao, *Nanoscale,* 2011**, 3**, 701.

14 A. A. Coelho, *TOPAS ACADEMIC. Brisbane: Australia* 2005.

15 H. J. Fan, M. Knez, R. Scholz, K. Nielsch, E. Pippel, D. Hesse, M. Zacharias and U. Gosele, *Nat. Mater.,* 2006**, 5**, 627.

16 S. Prasad and A. Paul, *Appl. Phys. Lett.,* 2007**, 90**, 233114.

17 (a) M. F. Berard and D. R. Wilder, *J. Appl. Phys.,* 1963**, 34**, 2318; (b) K. Ando, Y. Oishi, H. Hase and K. Kitazawa, *J. Am. Ceram. Soc.,* 1983**, 66**, C222.

18 (a) D. Yang, Z. Hou, Z. Cheng, C. Li and J. Lin, *Chem. Soc. Rev.,* 2015**, 44**, 1416; (b) R. Lv, S. Gai, Y. Dai, F. He, N. Niu and P. Yang, *Inorg. Chem.,* 2013**, 53**, 998; (c) D. Yang, X. Kang, P. a. Ma, Y. Dai, Z. Hou, Z. Cheng, C. Li and J. Lin, *Biomaterials,* 2013**, 34**, 1601.

19 X. Zhang, L. Zhou, Q. Pang, J. Shi and M. Gong, *J. Phys. Chem. C,* 2014**, 118**, 7591.

20 D. Yue, W. Lu, L. Jin, C. Li, W. Luo, M. Wang, Z. Wang and J. Hao, *Nanoscale,* 2014**, 6**, 13795.

21 (a) W. Zhou, J. Yang, J. Wang, Y. Li, X. Kuang, J. Tang and H. Liang, *Opt. Express,* 2012**, 20**, A510; (b) W. Zhou, Y. Li, R. Zhang, J. Wang, R. Zou and H. Liang, *Opt. Lett.,* 2012**, 37**, 4437.